ELSEVIER

Earth and Planetary Science Letters 195 (2002) 261–275

EPSL

www.elsevier.com/locate/epsl

Compaction creep of quartz sand at 400–600°C: experimental evidence for dissolution-controlled pressure solution

A.R. Niemeijer *, C.J. Spiers, B. Bos [1]

HPT Laboratory, Faculty of Earth Sciences, Utrecht University, P.O. Box 80.021, 3508 TA Utrecht, The Netherlands

Received 24 July 2001; received in revised form 13 November 2001; accepted 14 November 2001

Abstract

Intergranular pressure solution (IPS) is an important compaction and deformation mechanism in quartzose rocks, but the kinetics and rate-controlling process remain unclear. The aim of the present study is to test microphysical models for compaction creep by IPS against isostatic hot pressing experiments performed on quartz sand under conditions expected to favor pressure solution (confining pressure 300 MPa, pore water pressure 150–250 MPa, temperature 400–600°C). Microstructural observations revealed widespread intergranular indentation features and confirmed that intergranular pressure solution was indeed the dominant deformation mechanism under the chosen conditions. For porosities down to 15%, the mechanical data agree satisfactorily with a microphysical model incorporating a previously determined kinetic law for dissolution of loose granular quartz, suggesting that the rate-limiting mechanism of IPS was dissolution. The model also predicts IPS rates within one order of magnitude of those measured in previous experiments at 150–350°C, and thus seem robust enough to model sandstone compaction in nature. Such applications may not be straightforward, however, as the present evidence for dissolution control implies that the compositional variability of natural pore fluids may strongly influence IPS rates in sandstones.

Keywords: rocks; deformation; pressure solution; kinetics; sandstone; compaction; diagenesis

1. Introduction

Despite its importance as a compaction, deformation and fault healing mechanism in the upper crust [1–4], the rate-controlling mechanism and kinetics of intergranular pressure solution (IPS) in quartz are poorly constrained, mainly because of the extreme slowness of the process under laboratory conditions [2,5]. Nonetheless, microstructural evidence for the operation of IPS has been obtained in a number of experimental studies, as have crude rate data. The earliest such studies involved uniaxial (one-dimensional) compaction experiments on wet quartz sand at temperatures of 270–550°C, conducted by Renton et al. [6] and de Boer et al. [7]. These authors demonstrated slow compaction creep that accelerated towards

* Corresponding author. Tel.: +31-30-253-4976; Fax: +31-30-253-7725.
E-mail address: a.r.niemeijer@students.geo.uu.nl (A.R. Niemeijer).

[1] Present address: TNO TPD Materials Technology, Eindhoven, The Netherlands.

0012-821X/02/$ – see front matter
PII: S0012-821X(01)00593-3

higher temperature, higher effective pressure and finer grain size, though they did not systematically investigate these effects. From intergranular indentations they inferred that IPS was the dominant compaction mechanism, accompanied by grain scale cataclasis at the lower temperatures.

In densification experiments performed at 360°C, using an effective pressure of ~50 MPa and a variety of pore fluid compositions (pure water vs. 0.1–1.0 molar NaOH solution), Gratier and Guiguet [8] obtained convincing microstructural evidence for deformation by IPS. By inserting dissolution kinetics estimates for quartz into a theoretical model for IPS, they inferred that diffusion must have been rate controlling in their experiments. Schutjens [9] performed more systematic 1-D compaction creep experiments on wet quartz sand (40–100 μm) at temperatures of 250–350°C, using confining pressures of 20–30 MPa and an alkaline pore fluid ($Na_2SiO_3 \cdot 5H_2O$ added to achieve silica saturation) at a pressure of ~15 MPa. He too found grain indentations and contact truncations evidencing IPS, with grain cracking at lower temperatures. However, on the basis of the apparent activation energy for creep ($\Delta H \approx 60$–75 kJ/mol), Schutjens suggested that the rate-limiting IPS process was dissolution at grain contacts. In a single isostatic compaction experiment on fine-grained (4 μm) granular quartz, performed at a confining pressure of 300 MPa and a pore pressure of 200 MPa, but at much higher temperatures (927°C), Cox and Paterson [10] obtained compaction creep strain rates as high as 10^{-5}–10^{-6} s^{-1}. From grain contact microstructures, they concluded that this occurred by IPS, but did not investigate the effects of varying stress, temperature and grain size and did not consider the rate-controlling process. More recently, Dewers and Hajash [11] reported long-term isostatic compaction experiments performed on aeolian quartz sand (grain size 90–350 μm) at 150–200°C at a confining pressure of ~70 MPa and a pore fluid (pure water) pressure of ~35 MPa (effective pressure of ~35 MPa). Though the strains achieved were small (<10%), on the basis of mechanical, microstructural and chemical data, they inferred that pressure solution was again the dominant compaction mechanism, accompanied by time-dependent cataclasis particularly at lower temperatures. From the apparent activation energy for creep ($\Delta H \approx 73$ kJ/mol), and their finding that the pore fluid silica concentration increased with applied stress, Dewers and Hajash suggested that interface kinetics may have controlled IPS.

From these studies, it is clear that while IPS occurs at detectable rates in experiments on quartz at temperatures above ~150°C, systematic data on the effects of temperature, effective pressure and grain size on the rate of the process are sparse and the kinetics and rate-controlling mechanisms remain poorly understood. In this paper, we report isostatic compaction experiments performed on quartz sand at 400–600°C, a confining pressure of 300 MPa, pore fluid pressures of 150–250 MPa and using grain sizes of 30–100 μm, in an attempt to assess better the effect of these variables on volumetric strain rates by IPS. Our choice of stress and temperature conditions was expected to yield IPS strain rates which would be measurable on a time scale of 1–5 days and was based on extrapolations of previous data. Our study extends the previous 1-D compaction experiments of Schutjens [9] to higher temperatures and effective pressures, and to higher volumetric strains or lower porosities (down to ~10%). We chose the isostatic configuration rather than 1-D, because this rules out any effects of vessel wall friction or shear stress. The results obtained are compared with non-linear theoretical models for both reaction- and diffusion-controlled IPS in an attempt to identify the rate-controlling process and constrain better what this may be in nature.

2. Theoretical background

In a chemically closed system (no addition or removal of solid mass via long range transport in the pore fluid phase), compaction of a fluid-saturated granular aggregate by intergranular pressure solution (IPS) involves dissolution of solid material at stressed grain-to-grain contacts, diffusion of this material through the intergranular fluid into the open pores, followed by precipitation on free pore walls. The process is driven by differ-

ences in effective normal stress, hence normal component of solid chemical potential, between grain contacts and free pore walls [2,12,13]. If the pore fluid pressure acting on the free pore walls is P_f, the thermodynamic driving force (chemical potential difference) for transport between source (grain boundary) and sink (pore wall) sites is given:

$$\Delta\mu_n = \mu_{gb} - \mu_{pore} = (\sigma_n - P_f)\cdot\Omega \quad (1)$$

where μ_{gb} is the average chemical potential of the solid within a representative element of the grain contact, μ_{pore} is the chemical potential of the solid at pore wall sites, σ_n is the normal stress acting across the grain boundary element, P_f is the pore fluid pressure and Ω is the molar volume of the solid [2,3,5]. Under steady state conditions, this thermodynamic driving force drives the three serial processes of dissolution, diffusion and precipitation, such that the slowest kinetic step controls the overall deformation rate of the aggregate.

Making use of the relation between the chemical potential (μ) of a dissolved solid and its concentration (C) in an ideal solution ($\mu = \mu_0 + RT \ln C/C_0$), it is easily shown that the potential drop ($\Delta\mu_n$) between source and sink sites corresponds to a difference in solubility of the solid (ΔC) such that:

$$\Delta\mu_n = RT \ln\left(\frac{C_p + \Delta C}{C_p}\right) \approx RT\frac{\Delta C}{C_0} \quad (2)$$

Here R is the gas constant, T is absolute temperature, ΔC is the enhancement of the solubility of the solid within a stressed grain contact element relative to free pore wall sites, and C_p is the solubility of the solid at free pore wall sites. Neglecting minor deformation at the free grain surfaces, C_p will be approximately equal to the solubility (C_0) of the solid grains under purely hydrostatic reference conditions (pressure in solid and fluid = P_f).

Grain boundary diffusional IPS requires a grain boundary structure that allows fluid access despite high intergranular normal stresses. Two grain boundary models are well known in the literature, namely the adsorbed fluid film model [5,15] and the island-channel model [16,17]. For the development of a rate theory of IPS it is not important which grain boundary structure exists during the process, provided that the amplitude of any roughness and associated fluctuations in the Helmholtz free energy of the solid are small compared with grain contact length. Numerous authors [5,12,13,16–18] have published theoretically derived rate equations for IPS. Assuming that all of the driving force, $\Delta\mu_n$, is taken up in driving the rate-controlling processes of either dissolution at grain boundaries, diffusion within the grain boundary or precipitation on the pore walls, all of these models lead to essentially identical results. For compaction creep of a regular pack of spherical grains, this can be written [19]:

$$\dot{\varepsilon}_x = A_x\cdot Z_x(T)\cdot[B(\phi, \phi_0)\cdot P_e\cdot\Omega/(R\cdot T)]^n f_x(\phi, \phi_0)/d^p \quad (3)$$

Here $\dot{\varepsilon}$ is the volumetric strain rate (s^{-1}), x denotes dissolution, diffusion or precipitation control (x = s,d,p), the A_x are geometric constants, $Z_x(T)$ is a temperature-dependent kinetic coefficient for the relevant rate-controlling process, P_e is the applied effective pressure, $B(\phi,\phi_0)$ is a measure of the stress concentration at grain contacts due to aggregate structure, d is grain diameter and the $f_x(\phi,\phi_0)$ represent mechanism-specific functions of the ratio of instantaneous aggregate porosity (ϕ, %) to starting porosity (ϕ_0, %). The powers p and n take values of 3 and 1 respectively, when grain boundary diffusion is the rate-controlling process of IPS. When dissolution or precipitation is rate controlling, p is 1 and n reflects the order of the interface velocity vs. driving force relation (typically n = 1 for a rough interface, or 2 for spiral growth/dissolution; [20]). Note that the functions $B(\phi,\phi_0)$ and $f_x(\phi,\phi_0)$ respectively describe the progressive changes in grain contact area, and in transport path length and pore surface area, during ongoing compaction. For an assumed starting configuration of equi-dimensional spherical grains in a simple cubic (SC), a face centered cubic (FCC) or a body centered cubic (BCC) packing, B, f_x and hence the strain rate can be expressed as exact functions of ϕ and ϕ_0 as indicated in Eq. 3. However, compu-

tations of compaction by IPS, assuming an SC, FCC, BCC or random packing, predict B, f_x and strain rate vs. ϕ/ϕ_0 curves that approach single master curves at $\phi > 5\%$. For the purpose of comparing experimental trends with IPS theory, the quantity ϕ/ϕ_0 thus offers a useful way of measuring porosity reduction, since it, in theory, reduces the effect of varying initial porosity and packing on strain rate under otherwise fixed conditions.

In deriving Eq. 2 and hence Eq. 3, the approximation is made that $\ln(1+\Delta C/C_p) \approx \Delta C/C_p$, following the now almost standard assumption made by Rutter [5] that $\Delta C/C_p \ll 1$, i.e. assuming that the solubility enhancement at stressed grain boundaries is small. It is this approximation which leads to the linear relation between stress and strain rate widely considered characteristic of IPS. However, several workers have recently argued that the approximation is not valid for high grain contact stresses (small contact area, high B-values) and materials with large molar volume ([11], Rutter, personal communication). Indeed, order of magnitude estimates of the term ($B\sigma_e\Omega/RT$), for an SC pack, taking $B \geq 5$, show that the approximation is significantly in error for the conditions encountered in compaction tests on granular quartz. Following the analysis employed by previous workers [5,12,13,16–18] to obtain Eq. 3, but omitting the approximation $\Delta C/C_p \ll 1$, produces the result:

$$\dot{\varepsilon}_x = A_x \cdot Z_x(T)\left(\exp\left(\frac{B(\phi,\phi_0)\cdot P_e\cdot\Omega}{R\cdot T}\right)-1\right) \cdot f_x(\phi,\phi_0)/d^p \quad (4)$$

for the case that n is 1, i.e. for the case of diffusion-controlled IPS or of linear reaction-controlled IPS. A similar exponential form for the strain rate vs. stress relation for compaction is also given by Dewers and Hajash [11].

3. Experimental method

Our experiments consisted of isostatic compaction or hot pressing (HIPing) experiments carried out on wet quartz sand. The aim was to test the applicability of the above exponential models for IPS [4] by systematically varying effective pressure, temperature and grain size. The temperature range used was 400–600°C, the effective pressure 50–150 MPa, the confining pressure 300 MPa and the pore fluid pressure 150–250 MPa. The experiments were carried out using the same starting material as that used by Schutjens [9], namely milled and HF-rinsed quartz sand from the Miocene 'Bolderiaan' formation, Belgium [9]. We sieved this material into grain size fractions with initial grain sizes (d_i) of 28–37 μm, 45–75 μm and 100–125 μm.

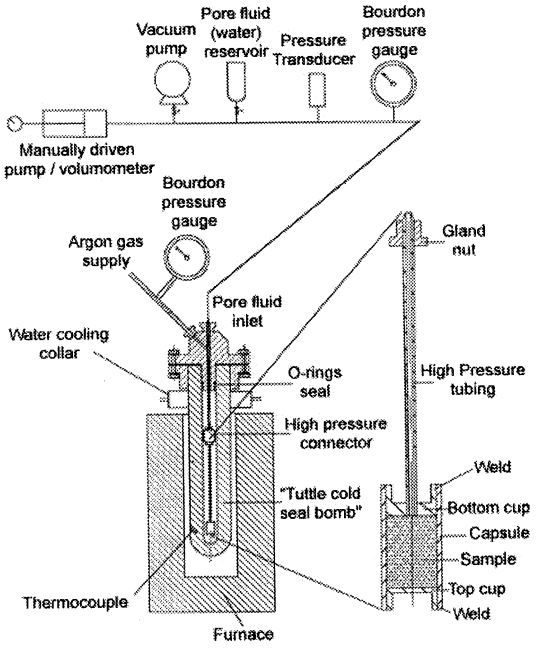

Fig. 1. Schematic diagram of the experimental apparatus with an enlargement showing the capsule/sample set-up.

3.1. Apparatus and procedure

Fig. 1 shows a schematic diagram of the apparatus used. It consists of a cold seal 'Tuttle bomb' pressurized with argon, plus an internal sample/capsule assembly linked to a pore fluid system, consisting of a vacuum pump, a reservoir and a volumetric pump. The pore fluid pressure was measured with a Bourdon-type pressure gauge (resolution ~1 MPa) in our earlier tests and later

using a pressure transducer (resolution ~0.2 MPa). The argon confining pressure was measured using a Bourdon gauge. The temperature of the sample was measured indirectly using a K-type thermocouple embedded in the bomb wall, with an error of ~2°C estimated from calibration runs.

In initiating each experiment, ~2 g of sand was loaded into the annealed copper capsule assembly via the initially open 'top cup' end (enlargement Fig. 1). The capsule was then sealed by pressing and welding in the copper 'top cup' (Fig. 1), producing a sample porosity of ~45–50%. The sample assembly was subsequently loaded into the Tuttle bomb and evacuated and flooded with water from the pore fluid reservoir. Each sample was then cold isostatically pressed (CIPed) at a confining pressure of 300 MPa under drained conditions for 30 min. This was done with the aim of producing a reproducible starting porosity and microstructure for the hot pressing stage (cf. [14,19]), and to minimize strain by grain rearrangement and contact cataclasis during HIPing (conducted at only 50–150 MPa). The confining pressure was subsequently reduced to ~140 MPa (depending on the desired test temperature) and the pore fluid pressure raised to ~135 MPa using the manually operated volumometer pump. The sample was then heated at ~15°C per min. During heating, the effective pressure was maintained as low as possible and was always <10 MPa. Note that any surface damage introduced into the grains by CIPing would be more or less entirely removed during heating, since significant surface dissolution is required to saturate the pore fluid with silica under the chosen test conditions. After attaining thermal equilibrium at the desired test temperature and confining pressure (300 MPa), the required effective pressure was applied and maintained by extracting fluid from the sample using the volumometer. The confining and pore fluid pressures were subsequently kept within ±5 MPa of the desired values. The minimum measurable fluid volume increment was ~2 μl. This corresponds to an absolute resolution in volumetric strain at room temperature of ~0.02%.

Experiments were terminated when the pore volume loss was no longer detectable via changes in pore fluid pressure. At this stage, the bomb was quenched using compressed air, at an average cooling rate of ~30°C per min. The indurated sample was then removed from the apparatus and capsule, and dried in an oven at 60°C for 24 h. The final porosity (ϕ_f) of the sample was measured by wrapping it in ultra-thin plastic

Table 1
List of experiments performed showing initial (pre-HIPing) porosities (ϕ_0), final porosities (ϕ_f), sieved grain sizes (d_i), final grain sizes (d_f) as determined by image analysis (linear intercept method) after the experiments, and isostatic pressing conditions

Sample number	T (°C)	d_i (μm)	d_f (μm)	P_c (MPa)	P_f (MPa)	P_e (MPa)	ϕ_0 (%)	ϕ_f (%)	Total strain (%)
D9	20	45–75	27.9 ± 19.3	300	~0.1	~300	30.31[a]	30.31	–
D15	500	45–75	10.2 ± 9.5	300	'dry'	300	29.96[a]	15.24	16.64
D17	500	45–75	14.9 ± 12.8	60	'dry'	60	27.17[a]	19.65	9.06
CPf3	500	45–75	47.1 ± 23.3	300	200	100	27.31[b]	12.71	16.70
CPf4	500	45–75	42.9 ± 24.9	300	150	150	29.39[b]	10.51	20.78
CPf5	500	45–75	40.5 ± 23.3	300	250	50	26.12[b]	16.60	11.35
CPf6	400	45–75	40.9 ± 25.0	300	200	100	25.14[b]	15.36	10.99
CPf7	600	45–75	43.2 ± 22.4	300	200	100	31.38[b]	9.70	23.86
CPf8[c]	500	28–35	11.7 ± 7.2	300	200	100	31.08[b]	14.65	19.21
CPf9	500	100–125	85.9 ± 43.9	300	200	100	24.51[b]	10.32	15.72

T denotes test temperature, P_c confining pressure, P_f pore fluid pressure and P_e the applied effective pressure. 'Dry' means no water added.

[a] Starting or pre-HIPing porosity measured under atmospheric conditions, i.e. after CIPing.

[b] Starting or pre-HIPing porosity calculated for loaded conditions from the final porosity and porosity change determined during HIPing.

[c] Fluid pressure measured with high pressure transducer.

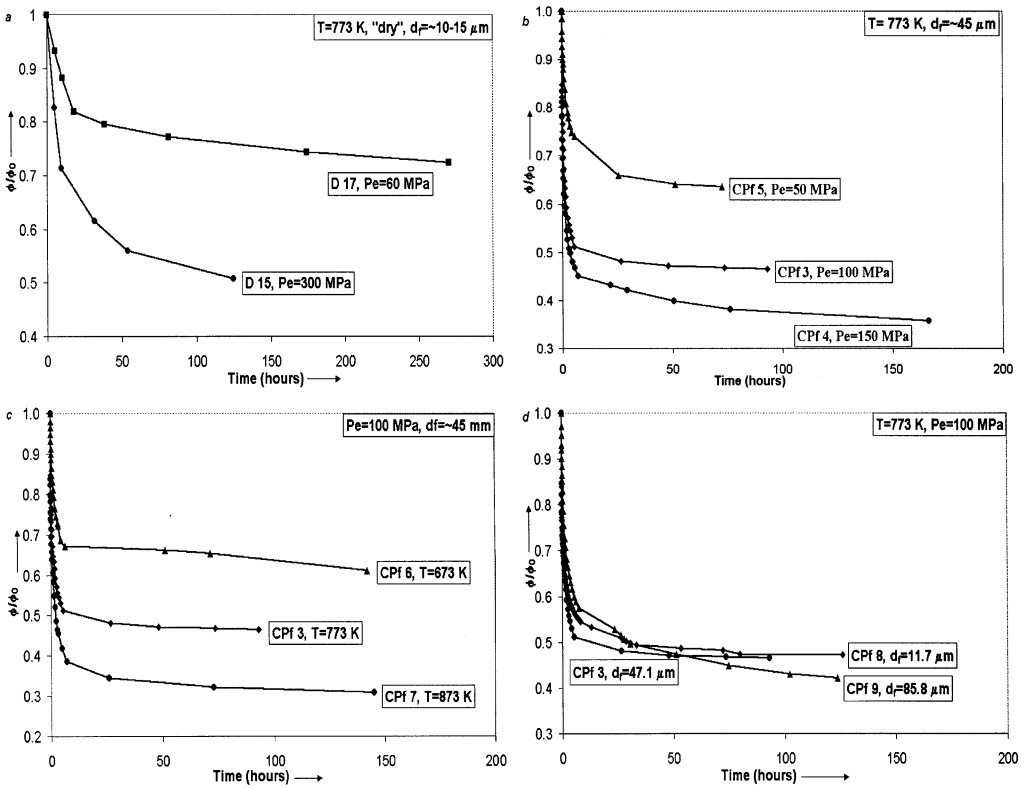

Fig. 2. Compaction creep curves in the form of ϕ/ϕ_0 vs. time plots. (a) Dry compacted samples. (b), (c) and (d) Wet compacted samples showing the influence of effective pressure, temperature and grain size, respectively.

film and determining its volume (*V*f) using the Archimedes method. The samples were finally impregnated with epoxy resin and sections were cut for optical and SEM study.

3.2. Data acquisition and processing

As indicated above, pore volume loss during the experiments was determined incrementally by measuring the volume of fluid extracted from the sample to maintain constant pore pressure. The measurements were accurately corrected for density changes associated with the cooling of the pore fluid during extraction, using appropriate *P-V-T* equations for water [21]. The 'starting porosity' (ϕ_0) of the sample, i.e. before HIPing at the test temperature, was calculated by adding the total amount of fluid expelled from the sample during HIPing to the final pore volume (ϕ_f, V_f) of the sample. The error introduced here, through the difference in the pore and sample volumes measured at room temperature and pressure compared to the post-HIPing volumes at test condition, can be estimated using bulk modulus values for sandstone (~ 2.5–7.5×10^{11} Pa [22]) and the volumetric thermal expansion coefficient of quartz (~ 4–5×10^{-5} K^{-1} [23]), and was found to be negligible. However, measurement of final porosity was problematic, since it was difficult to wrap the plastic film precisely around the sometimes irregular samples. Final porosity measurements were therefore repeated 10 times to obtain an average value. The resulting absolute standard error was around 0.5%. Taking all error sources into account, we estimate that the overall relative standard error in volume measurements was approximately 5%, implying an absolute standard error in the porosity measurements of less than

0.2%. Volumetric strain rates were calculated from our volume/porosity vs. time data using the two-point central difference method. Because considerable grain breakage was demonstrated during the CIPing stage of each test, the arithmetic mean grain size (d_f) of all samples was determined after testing by applying the linear intercept method to both reflected light and SEM backscatter images [24]. We have used this final mean grain size d_f in the analysis of our results.

3.3. Dry control runs

Control HIPing experiments on 'dry' sand fractions were performed in the same apparatus as the wet tests, but using fully sealed capsules with no added water (pore fluid system not connected). The 'dry' samples were first CIPed at 300 MPa for 30 min and their porosity determined at atmospheric pressure using the Archimedes method. The samples were then HIPed at 500°C and pore volume loss was measured periodically by removing the capsule from the bomb and re-determining its total (current) volume.

4. Results

4.1. Mechanical data

The complete set of experiments along with our data on the pre-HIPing or 'starting porosities' (ϕ_0), final porosities (ϕ_f) final grain sizes and total strains achieved are listed in Table 1. CIPing of the wet samples led to compaction from the initial porosity of 45–50% to ~30% (see CIPed only sample D9, Table 1). The HIPing curves obtained for all dry and wet samples are presented in Fig. 2a–d, in the form of ϕ/ϕ_0 vs. time plots. Normalized porosity ϕ/ϕ_0 is used following the reasoning, given in our explanation of Eqs. 3 and 4, that it

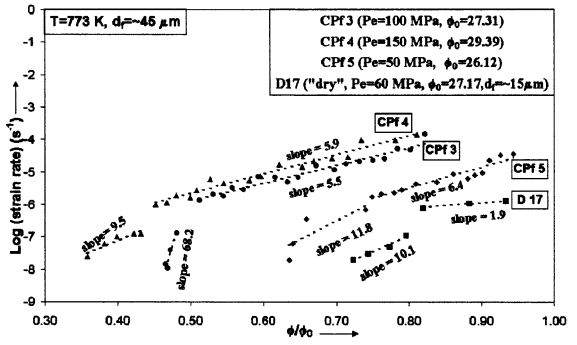

Fig. 3. Log (strain rate) vs. ϕ/ϕ_0 plots with linear best fits for 'dry' sample D17 and wet samples CPf3, CPf4, and CPf5 (varying effective pressures).

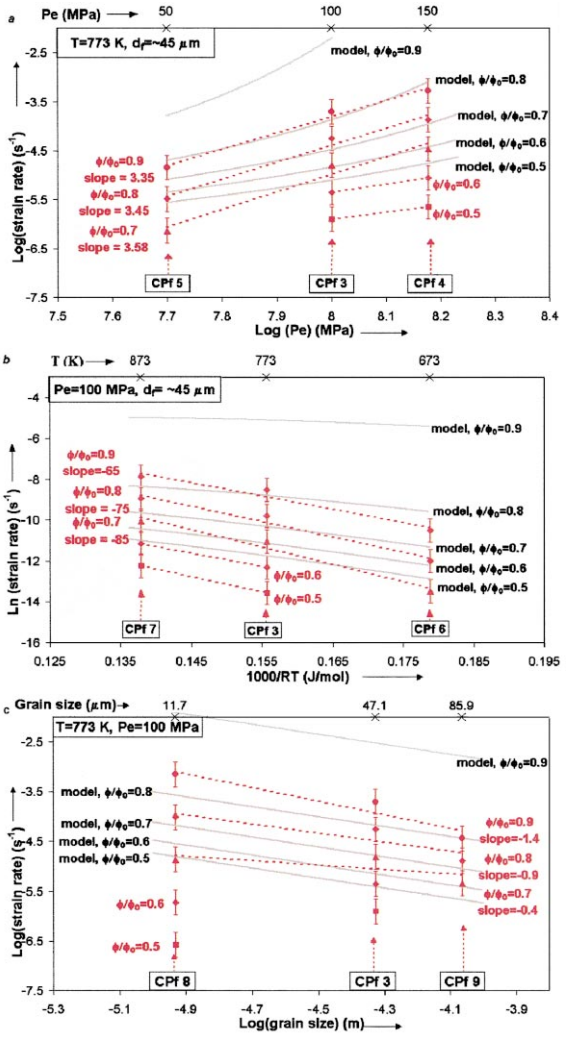

Fig. 4. Plots showing effects of (a) effective pressure, (b) temperature and (c) final grain size on experimentally determined compaction strain rates. Data sets (in red) represent experimental values obtained for fixed ϕ/ϕ_0. Red dotted lines are best fits obtained by linear regression analysis for individual ϕ/ϕ_0-values. Gray lines are the model predictions for the dissolution-controlled case.

Table 2
Coefficient and intercept parameter values determined by multiple linear regression fitting to the data shown in Fig. 4 and by averaging the individual linear regression fits shown in Fig. 4

Term	Multiple regression fit		Individual regression fits		
	Coefficient	Std error	Coefficient	Std error	Corr. Coeff.
$\ln(\varepsilon)$	–	±0.4432	–	±0.5399	–
Intercept	−70.3994	±3.4753	−79	–	–
$\ln(\sigma)$	3.0910	±0.1792	3.5	±0.25	0.97
$\ln(d_f)$	−0.5849	±0.0814	−0.9	±0.5	0.80
$1000/RT$	−77.5655	±4.3330	−75	±10	0.97
$\ln(10^{\phi/\phi_0})$	5.0650	±0.1717	5.2596	–	–

In both cases, a power law dependence of strain rate on P_e and d_f and an exponential dependence on $1/RT$ and ϕ/ϕ_0 was assumed. Fitting was carried out taking the natural logarithm of the strain rate as the independent variable. In the multiple regression analysis, the complete data set for the region $\phi/\phi_0 > \sim 0.55$ has been analyzed. The correlation coefficient in this case was 0.90.

forms a useful single measure of porosity when ϕ_0 is not constant. Fig. 2a demonstrates time-dependent compaction in the 'dry' HIPed samples plus increased compaction with increasing confining pressure. However the rates of dry compaction are very slow.

The starting porosity ϕ_0 of the wet samples (i.e. porosity before HIPing) varied from 24 to 31% (Table 1). These variations are probably the result of different heating times, effective pressure differences during heating and different sieved grain sizes (CPf8 and CPf9). HIPing of the wet samples led to much more rapid compaction than seen in the 'dry' samples, producing volumetric strains up to 24% and porosities as low as ∼10% after only 1–2 days (Table 1, Fig. 2b–d). Fig. 2b shows the compaction curves for wet samples HIPed at different effective pressures. Porosity reduction clearly increases with increasing effective pressure. Fig. 2c and d demonstrate that porosity reduction also accelerates with increasing temperature and with decreasing final grain size (at least for the early stages of compaction).

Fig. 3 shows typical strain rate vs. ϕ/ϕ_0 data for wet HIPed samples CPf3, 4 and 5. Note the near linear trends in the region $\phi/\phi_0 > 0.5$–0.6 ($\phi > 15\%$). Data for the dry HIPed sample D17 are added for comparison and demonstrate much slower creep rates (∼10 times). Such plots were used (by interpolation/extrapolation of the best fits) to construct graphs showing the dependence of strain rate ($\dot{\varepsilon}$) in the wet HIPed samples on effective pressure (P_e), temperature (T) and grain size (d_f) at constant normalized porosity (ϕ/ϕ_0) – see Fig. 4a–c. The slopes of the best fit trends (dashed lines) seen in the log–log plot of Fig. 4a (3.35–3.58) imply that the strain rate during HIPing is roughly proportional to the effective pressure raised to the power 3.5. Similarly, the Arrhenius fits of Fig. 4b yield slopes in the range −65 to −85, implying an apparent activation energy for creep of 75 ± 10 kJ/mol. The best fits seen in Fig. 4c show that the strain rate is relatively insensitive to grain size, decreasing with d_f raised to powers in the range -0.9 ± 0.5. The complete data set for the region $\phi/\phi_0 > \sim 0.55$ has been analyzed using multiple linear regression, assuming a power law dependence of strain rate on P_e and d_f and an exponential dependence on $1/RT$ and ϕ/ϕ_0. The results are shown in Table 2, along with the mean fit parameters obtained for the individual fits shown in Fig. 4a–c. Note that the two sets of fit parameters are mostly very similar.

4.2. Microstructural observations

Starting fractions of the Bolderiaan sand (>99% quartz) were described by Schutjens [9]. Our optical and SEM observations confirmed the quartz grains to be subangular to angular with surfaces characterized by triangular, pyramidal and sickel-shaped etch pits (0.1–0.5 μm). In about 5% of the grains, subparallel planar arrays of fluid inclusions were present, resembling healed intragranular microcracks.

Optical microscopy and SEM performed on

CIPed only material (sample D9, which underwent identical treatment to all wet HIPed samples prior to their wet HIPing stage) and on 'dry' HIPed samples (D15, D17) revealed qualitatively indistinguishable microstructures characterized by widespread transgranular and intragranular cracks, strongly reduced final grain size and sharp grain contact points (Fig. 5a). Quantitatively, however, the 'dry' HIPed samples were significantly finer grained as well as denser than the CIPed only sample (see Table 1). We found no microstructural evidence that dissolution/precipitation processes were active in these samples.

The final mean grain size of the wet HIPed samples was reduced compared to the starting sand fractions, but much less than in the case of cold compacted or 'dry' HIPed samples (Table 1). In the wet HIPed samples (Fig. 5b,c), fewer fines and fewer cracks were observed than in CIPed only material, suggesting that many of the finest cataclastic fragments seen in the cold-pressed material dissolved during pre-HIP heating and/or HIPing itself, and that some cracks may have healed. All wet HIPed samples show a relatively dense microstructure (Fig. 5c). Minor undulatory extinction is visible optically, but the total fraction of grains showing this is less than 5%. All wet samples show tightly fitting, often micro-sutured grain boundaries and concavo-convex grain to grain contacts (indentations and truncations, Fig. 5b,c). We observed only a few intragranular fractures associated with well-fitting or indented grain contact, suggesting that interaction between fracturing and pressure solution [25] did not play an important role in our experiments.

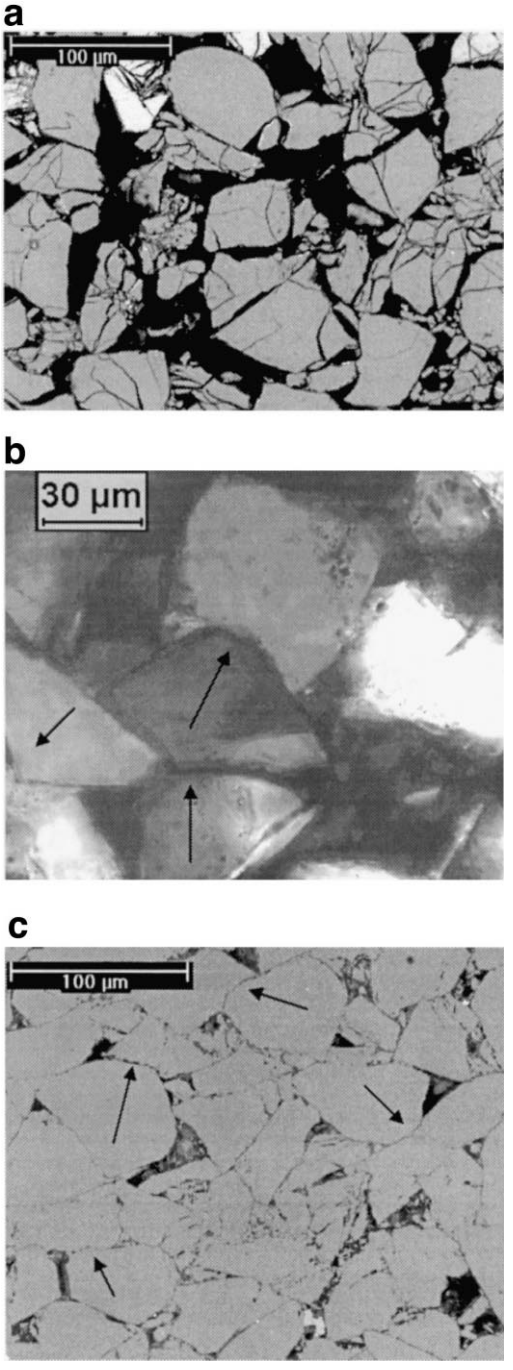

→

Fig. 5. (a) SEM backscatter image of cold isostatically pressed sample D9 (wet CIPed at $P_c = 300$ MPa for 0.5 h, $P_f = 0.1$ MPa, $d_f = 27.9$ μm and $\phi = 30.53\%$). (b) Transmission optical micrograph of sample CPf4 with crossed polarizers ($P_e = 150$ MPa, $T = 773$ K (500°C), $d_f \approx 45$ μm and $\phi_f = 10.51\%$). (c) SEM backscatter image of sample CPf5 ($P_e = 50$ MPa, $T = 773$ K (500°C), $d_f \approx 45$ μm and $\phi_f = 16.60\%$). Note the widespread indentation features in (b) and (c) (indicated by the arrows).

5. Discussion

5.1. Deformation mechanisms in the 'dry' compacted samples

Our microstructural observations on the 'dry' HIPed samples (D15, D17, Table 1) suggest that the recorded compaction (Fig. 2a) involved mainly grain fracturing. Intergranular rearrangements must also have taken place. The slow but significant time-dependent component of compaction in the 'dry' HIPed samples (Figs. 2a and 3) suggests that dislocation creep, diffusion creep or subcritical cracking mechanisms contributed. However, no evidence was found from microstructural observations for significant dislocation or diffusion creep. We conclude that some form of subcritical cracking mechanism was responsible for most of the strain and porosity reduction measured.

5.2. Deformation mechanisms in the wet compacted samples

Like the dry HIPed samples, the microstructure of wet material CIPed at room temperatures shows microcracking and strong grain size reduction ($d_f \approx 28$ μm) compared with the starting fractions (60 ± 15 μm). By contrast, the wet HIPed samples show only modest grain size reduction ($d_f \approx 45$ μm, Table 1). In addition these samples exhibit numerous truncated and concavo-convex grain to grain contacts (indentations) as well as sutured and tightly fitting grain boundaries, providing evidence for the operation of intergranular pressure solution [3,17]. However, the mechanical data for the wet HIPed samples indicate a power law stress dependence of creep rate, with a power (n) much larger than the value of 1 predicted by conventional models for pressure solution (Eq. 3). The observed n-values (~ 3.5) are closer to the stress exponents inferred for dislocation creep in quartzite ($2 \leq n \leq 4$, [26–28]). On the other hand, we found an apparent activation energy of $\sim 75 \pm 10$ kJ/mol in our experiments, whereas dislocation creep in wet quartz is characterized by values of 120–167 kJ/mol [26,27,29]. Moreover, we found an inverse grain size dependence of strain rate, whereas dislocation creep is grain size insensitive [26]. These considerations rule out dislocation creep as the dominant deformation mechanism in our wet HIPing experiments.

Another time-dependent mechanism that could have operated in our wet HIPed samples is stress corrosion cracking accompanied by intergranular sliding/rearrangement. As already discussed, however, grain size reduction was less pronounced than in the CIPed only and 'dry' HIPed samples. Moreover, stress corrosion crack growth velocity depends on stress in a highly non-linear way, with power law stress exponent values > 8 [30]. Stress corrosion cracking plus intergranular sliding is therefore unlikely to have been an important mechanism in our wet HIPing experiments. We found no evidence for micro-scale cracking/crushing and subsequent dissolution within grain contacts, though such a process cannot be ruled out particularly in the early part of the experiments.

From the above, we conclude that compaction in our wet HIPed samples was most likely dominated by IPS, presumably with intergranular sliding accomodation. The fact that the dependence of compaction rate on final grain size (d_f) can be described by a power law with an exponent of -0.9 ± 0.5 (Fig. 4c, Table 2), rather than the value of -3 expected for diffusion-controlled IPS, renders it unlikely that diffusion was rate limiting. Moreover, the apparent activation energy found in this study is much higher than typical values for diffusion (15–25 kJ/mol, [31]), whereas it falls exactly in the range characterizing quartz dissolution/precipitation kinetics [32], suggesting that pressure solution was interface reaction controlled in the present experiments. The fact that the stress sensitivity of strain rate (n-value) observed in our wet HIPing tests is significantly larger than 1 can potentially be explained by the exponential (rather than linear) stress dependence predicted by Eq. 4 for IPS under conditions of high grain contact stress. Several previous experimental studies of IPS in quartz [9,11] also show stress exponents larger than 1. We address this further below.

5.3. Comparison with theoretical model

To gain further insight into the rate-controlling

mechanism of IPS in our wet HIPing experiments, we now compare our results with the non-linear microphysical models for compaction by IPS represented in Eq. 4. To this end, we inserted the kinetic 'law' for quartz dissolution given by Rimstidt and Barnes [32] into the creep model for the dissolution-controlled case ($x = s$ in Eq. 4). We focus on the dissolution-controlled case because, for the small grain contact vs. pore wall areas relevant for the present experiments, insertion of precipitation kinetics laws [32] or reasonable values of the grain boundary diffusive transport coefficient Z_d (e.g. from [8,16,33]) into Eq. 4 predicts much faster creep, so that dissolution control is predicted. Note that $Z_d = DC\delta$, where D is the diffusivity of dissolved solid in the grain boundary fluid phase, C is its solubility and δ is the average thickness of the grain boundary fluid [2,4,18]. In incorporating the dissolution law of Rimstidt and Barnes into Eq. 4, we used their value for the dissolution rate constant k^+ (given by them in mol/m^{2}s) times the molar volume as the velocity of dissolution of grain surface in (m/s) for a driving force of 1 RT ($Z_s = k^+\Omega$ in Eq. 4). For an SC grain packing this yields:

$$\dot{\varepsilon} = 6\cdot\Omega \times 10^{(1.174-0.002028\cdot T-4158/T)}\cdot \left[\exp\left(B\cdot\frac{P_e\cdot\Omega}{R\cdot T}\right)-1\right]\cdot\frac{f_s(\phi,\phi_0)}{d} \quad (5a)$$

with

$$f_x = \left(\frac{100-\phi_0}{100-\phi}\right) \quad (5b)$$

and

$$B = \frac{d^2}{\pi}\cdot f_x\cdot\left[R_i^2-\frac{d^2}{4}(f_x)^{2/3}\right]^{-1} \quad (5c)$$

where d is the grain diameter (m), P_e is the applied effective pressure (Pa), porosities are in % and R_i is the instantaneous grain (pore wall) radius. This is given by the root of the equation:

$$\left(\frac{d}{2}\right)^3 - 2R_i^3 + \left(\frac{3}{2}R_i\right)^2\cdot\left[\frac{f_s}{4}\right]^{4/3} - \frac{3}{128}\cdot(f_s)^4 = 0 \quad (6)$$

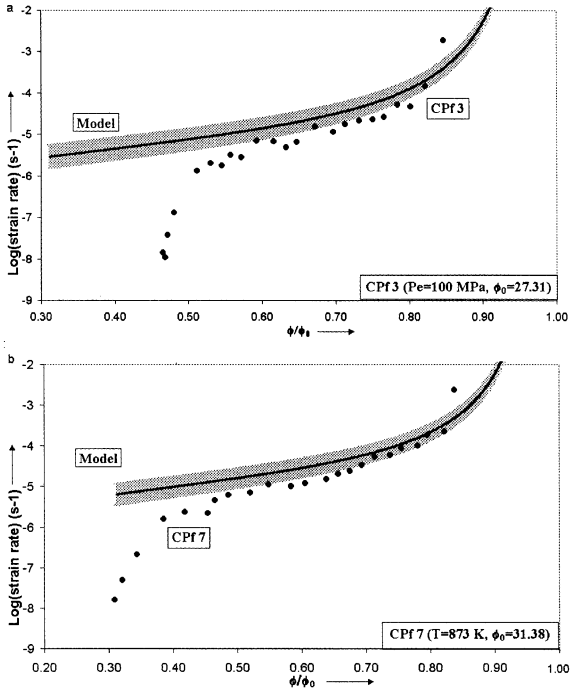

Fig. 6. Log strain rate vs. (ϕ/ϕ_0) curves comparing the experimental data of (a) sample CPf3, and (b) sample CPf7, with our microphysical model. The width of the band reflects a relative range in log strain rate of ±5%.

which is easily solved numerically. Note that in inserting the rate law of Rimstidt and Barnes [32] into Eq. 4, we assume that their dissolution law for free quartz surfaces also applies to a wetted grain boundary zone. Provided that dissolution is the dominant dissipative process operating within grain contacts (as opposed to plastic, frictional or acoustic dissipation), the non-equilibrium thermodynamic theory of Lehner [12] implies that this assumption is reasonable.

Fig. 6a,b compare the compaction creep rate vs. normalized porosity curves predicted by Eqs. 5a,b,c and 6), for the conditions of typical experiments (CPf3 and CPf7), with the corresponding experimental data. The model yields reasonable agreement with the experimental data at normalized porosities $\phi/\phi_0 > 0.5$ ($\phi \approx 15\%$), though it tends to overestimate the strain rate notably at lower porosity. If IPS is indeed the dominant deformation mechanism at high porosities, there could be several explanations for the sharp de-

crease in measured strain rates at $\phi/\phi_0 \approx 0.5$. First, there could be a change in rate-controlling mechanism from say dissolution to grain boundary diffusion-controlled IPS, as the grain contact structure evolves to a tighter 'fit' and larger area with increasing strain, or perhaps to precipitation control as pore wall area decreases. A second possibility is that there is a completely different evolution of mean grain contact geometry than embodied by the model. However, this should lead to a more gradual change in strain rate than observed. The abrupt change might otherwise be due to internal healing of the grain boundary structure, reducing the mean grain boundary fluid thickness or connectivity, or to contact overgrowth by neck growth [13]. Yet another explanation might lie in dissolution of copper from the capsule. The fact that the abrupt change in strain rate occurred in all experiments after ~ 12 h might correlate with a critical concentration of copper being reached after this period. The presence of dissolved copper strongly hinders dissolution rates of quartz [34–36] and thus may cause a strong decrease in IPS rate.

Focusing now on the main body of our experimental data, i.e. that obtained in the higher porosity regime ($\phi > \sim 15\%$ or $\phi/\phi_0 > \sim 0.5$), we have superposed our model predictions for dissolution-controlled IPS (Eqs. 5a,b,c and 6) onto these results (see Fig. 4a–c). Comparing behavior for individual values of ϕ/ϕ_0, the predictions of the model show similar trends and mostly fall within a half to one order of magnitude of the experimental data in absolute terms. Best agreement is seen regarding the stress sensitivity of the compaction rate (see trends at fixed ϕ/ϕ_0 in Fig. 4a plus best fit slopes in Table 2). With reference to Table 2, the grain size sensitivity of strain rate averaged over the individual fits of Fig. 4c also agrees favorably with the model, though the multiple regression fit agrees less well and we cannot eliminate the possibility that dissolution of fines produced in the CIPing stage may have influenced the observed grain size dependence. The model does tend to overestimate strain rate towards lower temperatures, lower effective pressures and higher porosities. Moreover, the temperature sensitivity of strain rate predicted by the model is lower than observed in the experiments. Note, however, that the dissolution kinetics data of Rimstidt and Barnes [32] were determined for the range 20–300°C, so that extrapolation to our conditions might lead to significant error in absolute rate and temperature sensitivity. Viewed overall, we feel that the model yields reasonable agreement with our measured creep rates and general trends, suggesting that compaction in our experiments was due to dissolution-controlled IPS, at least for porosities down to $\sim 15\%$.

5.4. Comparison with previous work

We now compare our experimental results and model predictions with previous data on IPS in pure quartz sands. We justify consideration of data obtained in both 1-D and isostatic compaction experiments on the grounds that our IPS model takes identical forms for both configurations, differing only by a numerical factor of 2–3. Strong effects of compaction mode seen in soil mechanics [37] are therefore not expected when IPS dominates. We begin by recalling that Schutjens [9] inferred dissolution to be the rate-controlling mechanism of IPS in his 1-D tests done at 250–350°C and 15 MPa effective pressure using alkaline pore fluids. Both the temperature and stress sensitivity of compaction rate found ($\Delta H = 67$ kJ and $2 \leq n \leq 4$) were similar to those seen in our experiments, though Schutjens found no systematic grain size effect. The activation energy for creep (73 kJ/mol) found by Dewers and Hajash [11] in their isostatic tests likewise resembles our value and suggests that interface kinetics controlled compaction by IPS. The non-linear dependence of strain rate on stress which they observed also resembles our result, but the sensitivity to grain size that they report was higher ($\dot{\varepsilon} \propto d^{-p}$ with $p = 2.3$). This may reflect differences in starting porosity ϕ_0 between the different grain size fractions used by Dewers and Hajash (hence the effect of their fitting parameter, ε_0), since in contrast to our approach they did not pre-press their samples to obtain a reproducible starting state.

Fig. 7 shows a quantitative comparison of our dissolution-controlled model (Eqs. 5a,b,c and 6)

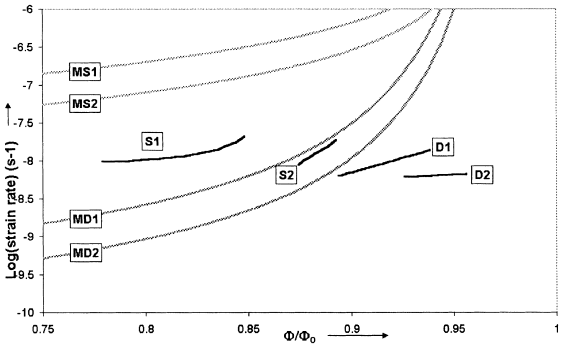

Fig. 7. Log strain rate vs. (ϕ/ϕ_0) curve comparing the experimental data of Schutjens [9] and Dewers and Hajash [11] with our microphysical model. S1: Schutjens [9], $T=623$ K (350°C), $P_e=15$ MPa, $d=90$ μm, data reproduced from strain–time plot. MS1: Microphysical model corresponding to conditions of S1. S2: Schutjens [9], $T=523$ K (250°C), $P_e=15$ MPa, $d=25$ μm, data reproduced from strain–time plot. MS2: Microphysical model corresponding to conditions of S2. D1: Dewers and Hajash [11], $T=423$ K (150°C), $P_e=35$ MPa, $d=105$ μm, data reproduced from empirical strain–time equation. MD1: Microphysical model corresponding to conditions of D1. D2: Dewers and Hajash [11], $T=423$ K (150°C), $P_e=35$ MPa, $d=215$ μm, data reproduced from empirical strain–time equation. MD2: Microphysical model corresponding to conditions of D2.

with empirical fits taken from Schutjens [9] and from Dewers and Hajash [11] for the range 150–350°C. Dewers and Hajash quote only an initial porosity of 35% in their micrograph captions, so we have assumed that this was the starting porosity in their experiments. Our model predicts creep rates which are about ~10 times faster than obtained in the previous 1-D and isostatic experiments, compared with 3–10 times faster than obtained in our isostatic tests. Similar agreement is obtained with two isostatic experiments on pure quartz sand at 400°C and 70 MPa effective pressure (P4, P7) recently reported by Rutter and Wanten [37]. We therefore infer that compaction of quartz by IPS is probably dissolution controlled across the entire range of 150–600°C.

5.5. Implications

Our findings suggest that IPS rates in granular quartz are controlled by the dissolution reaction down to a porosity of ~15% at 400–600°C and effective pressures of 50–150 MPa. Since the activation energy for quartz dissolution (~70 kJ/mol, [32]) is expected to be higher than that for diffusion in wetted grain boundaries (15–25 kJ/mol, [31]), then, unless diffusion at lower temperatures is much slower than currently thought [8,16,33], pressure solution rates in quartz rocks at temperatures below 600°C and porosities above ~15% should be controlled by the rate of dissolution. This implies that our model should be crudely applicable to predict IPS rates in natural sandstone formations with porosities >15%. Note, however, that since pore fluid chemistry strongly influences dissolution/precipitation rates in quartz [9,32,34–36], the composition of the pore fluid in sandstones may turn out to play the key role in determining IPS compaction rates, either slowing them down (e.g. Al^{3+}, Fe^{3+}, Zn^{2+}, Cu^{2+}, [34]) or speeding them up (e.g. Na^{+}, K^{+}, Li^{+}, Mg^{2+}, [34]). Further work on such effects is clearly needed, preferably using finer grain sizes and lower effective pressures than in the present study to further reduce any effects of cataclasis. For typical upper crustal conditions (depth 2 km, lithostatic pressure 50 MPa, fluid pressure 20 MPa, temperature 60–70°C, starting porosity 30–35%), the present dissolution-controlled IPS model predicts that sandstones with a grain size of 300 μm and a porosity of 20% will compact at strain rates of 10^{-13} to 10^{-12} s^{-1}. Our multiple regression fit predicts rates about one order lower.

6. Conclusions

1. From our mechanical data and microstructural observations we infer that the dominant compaction mechanism in our wet, hot-pressed samples at temperatures of 400–600°C and effective pressures of 50–150 MPa was intergranular pressure solution, though we cannot eliminate a minor contribution of cataclastic processes in the early stages of our tests.
2. A microphysical model incorporating an independently determined dissolution rate law with a non-linear (non-simplified) strain rate vs. driving force (stress) relation was compared with our data, as well as with previous experimental data for the temperature range 150–

600°C and the effective pressure range 15–150 MPa. The fit of our model to our own experimental data was surprisingly good for porosities higher than 15%, indicating that the rate-controlling mechanism of IPS was quartz dissolution at grain contacts. The fit was poor for lower porosities where measured rates slowed dramatically, possibly because of a change in rate-controlling mechanism, grain boundary healing or copper ions entering the pore fluid from the sample capsules. Predicted rates were 3–10 times faster than the compaction rates we measured and ~10 times faster than previous data.

3. The stress sensitivity of strain rate (n-values) of 3–4, which we found in our experiments, matched our non-linear IPS model prediction well and supports the notion that pressure solution in quartz needs not be linear viscous, when grain contact stresses are high.
4. Our dissolution-controlled model thus seems to give a robust order of magnitude description of quartz sand compaction by IPS, down to porosities of ~15%, and offers a basis to model compaction rates of quartz sandstones down to such porosity values. It is important to note, however, that pore fluid contamination might drastically slow down or accelerate the IPS process in nature depending on the ions present. More experimental work is needed on such effects, preferably using sufficiently fine grain sizes and low effective pressures to eliminate completely any effects of cataclasis.

Acknowledgements

We thank G. Kastelein for constructing our apparatus and P. van Krieken and E. de Graaff for further technical support. We also thank E.H. Rutter and A. Hajash for helpful reviews. *[RV]*

References

[1] C.L. Angevine, D.L. Turcotte, M.D. Furnish, Pressure solution lithification as a mechanism for the stick-slip behavior of faults, Tectonics 1 (1982) 151–1601.
[2] E.H. Rutter, Pressure solution in nature, theory and experiment, J. Geol. Soc. Lond. 140 (1983) 725–740.
[3] R. Tada, R. Siever, Pressure solution during diagenesis, Annu. Rev. Earth Planet. Sci. 17 (1989) 89–118.
[4] S.H. Hickman, B. Evans, Growth of grain contacts in halite by solution-transfer: Implications for diagenesis, lithification, and strength recovery, in: B. Evans, T.-f. Wong (Eds.), Fault Mechanics and Transport Properties of Rocks, Academic Press, London, 1992, pp. 253–280.
[5] E.H. Rutter, The kinetics of rock deformation by pressure solution, Philos. Trans. R. Soc. Lond. A 283 (1976) 203–219.
[6] J.J. Renton, M.T. Heald, C.B. Cecil, Experimental investigation of pressure solution of quartz, J. Sediment. Petrol. 39 (1969) 1107–1117.
[7] R.B. de Boer, P.J.C. Nagtegaal, E.M. Duyvis, Pressure solution experiments on quartz sand, Geochim. Cosmochim. Acta 41 (1977) 257–264.
[8] J.P. Gratier, R. Guiget, Experimental pressure solution-deposition on quartz grains: the crucial effect of the nature of the fluid, J. Struct. Geol. 8 (1986) 845–856.
[9] P.M.T.M. Schutjens, Experimental compaction of quartz sand at low effective stress and temperature conditions, J. Geol. Soc. Lond. 148 (1991) 527–539.
[10] S.F. Cox, M.S. Paterson, Experimental dissolution-precipitation creep in quartz aggregates at high temperatures, Geophys. Res. Lett. 18 (1991) 1401–1404.
[11] T. Dewers, A. Hajash, Rate equations for water-assisted compaction and stress induced water-rock interaction in sandstones, J. Geophys. Res. 100 (1995) 13093–13112.
[12] F.K. Lehner, Thermodynamics of rock deformation by pressure solution, in: D.J. Barber, D. Meredith (Eds.), Deformation Processes in Minerals, Ceramics and Rocks, Unwin Hyman, London, 1990, pp. 296–333.
[13] F.K. Lehner, A model for intergranular pressure solution in open systems, Tectonophysics 245 (1995) 153–170.
[14] C.J. Spiers, R.H. Brzesowsky, Densification behaviour of wet granular salt: theory vs experiment, in: H. Kakihana, H.R. Hardy, Jr., T. Hoshi, K. Toyokura (Eds.), Seventh Symposium on Salt, vol. 1, Elsevier Science, Amsterdam, 1993, pp. 83–92.
[15] F. Renard, P. Ortoleva, J.P. Gratier, Pressure solution in sandstones influence of clays and dependence on temperature and stress, Tectonophysics 280 (1997) 257–266.
[16] R. Raj, Creep in polycrystalline aggregates by mass transport through a liquid phase, J. Geophys. Res. 87 (1982) 4731–4739.
[17] C.J. Spiers, P.M.T.M. Schutjens, Densification of crystalline aggregates by fluid phase diffusional creep, in: D.J. Barber, P.G. Meredith (Eds.), Deformation Processes in Minerals, Ceramics and Rocks, Unwin Hymann, London, 1990, pp. 334–353.
[18] I. Shimizu, Kinetics of pressure solution creep in quartz theoretical considerations, Tectonophysics 245 (1995) 121–134.
[19] S. de Meer, C.J. Spiers, Uniaxial compaction creep of wet gypsum aggregates, J. Geophys. Res. 102 (1997) 875–891.

[20] A.E. Nielsen, Mechanism and rate laws in electrolyte crystal growth from aqueous solution, in: J.A. Davis, K.Y. Hayes (Eds.), Geochemical Processes at Mineral surfaces, ACS Symposium Series vol. 323, 1986, pp. 600–614.
[21] C. Burnham, J.R. Holloway, N.F. Davis, Thermodynamic properties of water to 1,000°C and 10,000 bars, Geological Society of America Special Paper vol. 132, 1969, 96 pp.
[22] F. Birch, Compressibility; elastic constants, in: S.P. Clark, Jr. (Ed.), Handbook of Physical Constants, rev. edn., Geological Society of America Memoir vol. 97, 1966, pp. 97–173.
[23] B.J. Skinner, Thermal expansion, in: S.P. Clark, Jr. (Ed.), Handbook of Physical Constants, rev. edn., Geological Society of America Memoir vol. 97, 1966, pp. 75–97.
[24] J.-H. Han, D.-Y. Kim, Analysis of the proportionality constant correlating the mean intercept length to the average grain size, Acta Metall. Mater. 43 (1995) 3185–3188.
[25] J.P. Gratier, F. Renard, P. Labaume, How pressure solution creep and fracturing process interact in the upper crust to make it behave in both a brittle and viscous manner, J. Struct. Geol. 21 (1999) 1189–1197.
[26] F.C. Luan, M.S. Paterson, Preparation and deformation of synthetic aggregates of quartz, J. Geophys. Res. 97 (1992) 301–320.
[27] G. Hirth, J. Tullis, Dislocation creep regimes in quartz aggregates, J. Struct. Geol. 14 (1992) 145–159.
[28] G.C. Gleason, J. Tullis, A flow law for dislocation creep of quartz aggregates determined with the molten salt cell, Tectonophysics 247 (1995) 1–23.
[29] P.S. Koch, J.M. Christie, A. Ord, R.P. George Jr., Effect of water on the rheology of experimentally deformed quartzite, J. Geophys. Res. 94 (1989) 13975–13996.
[30] B.K. Atkinson, P.G. Meredith, The theory of subcritical crack growth with applications to minerals and rocks, in: B.K. Atkinson (Ed.), Fracture Mechanics of Rock, Academic Press, London, 1989, pp. 111–166.
[31] S. Nakashima, Diffusivity of ions in pore water as a quantitative basis for rock deformation rate estimates, Tectonophysics 245 (1995) 185–203.
[32] J.D. Rimstidt, H.L. Barnes, The kinetics of silica-water reactions, Geochim Cosmochim. Acta 44 (1980) 1683–1699.
[33] J.R. Farver, R.A. Yund, Measurement of oxygen grain boundary diffusion in natural, fine grained, quartz aggregates, Geochim. Cosmochim. Acta 55 (1991) 1597–1607.
[34] P.M. Dove, J.D. Rimstidt, Silica-water interactions, Rev. Mineral. 29 (1994) 259–308.
[35] R. Iler, The Chemistry of Silica, Wiley, New York, 1979.
[36] P.M. Dove, The dissolution kinetics of quartz in aqueous mixed cation solutions, Geochim. Cosmochim. Acta 63 (1999) 3715–3727.
[37] E.H. Rutter, P.H. Wanten, Experimental study of the compaction of phyllosilicate-bearing sand at elevated temperature and with controlled pore water pressure, Sediment. Res. 70 (2000) 107–116.